scientific reports

Check for updates

OPEN

Plasma-activated solutions reverse chronic deltamethrin exposure induced intestinal injury via rebalancing redox homeostasis and counteracting cellular senescence

Xiaoyuan Deng[1,6], Tuanhe Sun[1,2,6], Siyi Wang[1], Kaijie Ren[1], Tianhao Min[1], Yuyi Ma[1], Yuanchang Peng[1], Xueni Wang[3], Bo Zhang[1,2], Yanglong Nan[1], Shiyao Tong[1], Yuanyuan Liu[1], Wei Wang[4], Yong Zhang[1], Yong Yang[5], Kang Li[1], Chengxue Dang[1], Hao Zhang[1]✉ & Kun Zhu[1]✉

Deltamethrin (DLM), a widely used pesticide, poses chronic exposure risks. Previous studies have shown its role in inducing intestinal mucosal barrier impairment. Meanwhile, plasma-activated solutions (PAS) ameliorate Dextran Sulfate Sodium (DSS)-induced colitis, primarily through the regulation of redox homeostasis. Building upon these findings, to further investigate the therapeutic potential of PAS against DLM-induced injury, we establish a chronic DLM exposure model in female BALB/c mice with concurrent free access to PAS. Intestinal tissues and serum are collected for H&E staining and measurement of serum inflammatory factors to assess inflammatory response. Immunofluorescence staining are used to detect intestinal injury and senescence. Reactive Oxygen Species (ROS) staining and glutathione (GSH) assays are performed to evaluate redox homeostasis. Results confirm that PAS effectively counteract chronic DLM-induced intestinal impairment, manifesting as restored body weight, decreased Disease Activity Index (DAI) scores, reduced apoptosis of intestinal epithelium and diminished inflammatory cell infiltration. To identify the key active component in PAS responsible for this therapeutic effect, A nitrogen-free PAS generator is used to produce nitric oxide-depleted PAS. Results show that after eight weeks of Nitro-Free PAS treatment, the therapeutic benefits are significantly weakened or disappeared. PAS mitigate chronic DLM induced intestinal impairment by rebalancing redox homeostasis, counteracting cellular senescence and restoring cell cycle progression. This therapeutic effect is mediated by reactive nitrogen species (RNS) within PAS.

Keywords Deltamethrin, Plasma-activated solutions, Intestinal mucosal barrier impairment, Redox homeostasis, Cellular senescence

Abbreviations

DLM	Deltamethrin
PAS	Plasma-activated solutions
DSS	Dextran sulfate sodium
ROS	Reactive oxygen species
RNS	Reactive nitrogen species
RONS	Reactive oxygen and nitrogen species

[1]Department of Surgical Oncology, The First Affiliated Hospital of Xi' an Jiaotong University, Xi'an 710061, Shaanxi, China. [2]State Key Laboratory of Electrical Insulation and Power Equipment, School of Electrical Engineering, Xi'an Jiaotong University, Xi'an 710049, Shaanxi, China. [3]Department of Hepatobiliary Surgery, The First Affiliated Hospital of Xi'an Jiaotong University, Xi'an 710061, Shaanxi, China. [4]Department of Obstetrics and Gynecology, The First Affiliated Hospital of Xi'an Jiaotong University, Xi'an 710061, Shaanxi, China. [5]Xi'an Analytical and Monitoring Centre for Agri–food Quality Safety, Xi'an 710077, China. [6]Xiaoyuan Deng and Tuanhe Sun contributed equally to this work. ✉email: hao.zhang@mail.xjtu.edu.cn; dr.zhkun@mail.xjtu.edu.cn

GSH	Glutathione
DAI	Disease activity index
CAP	Cold atmospheric plasma
N-free PAS	Nitrogen-free PAS
OH	Hydroxyl radicals
O_2^-	Superoxide anions
O_3	Ozone
NO	Nitric oxide
NO2	Nitrogen dioxide
$ONOO^-$	Peroxynitrite
SA-β-gal staining	β-galactosidase staining

Pyrethroids account for approximately 38% of the global insecticide market share in 2015, ranking as the second-largest category[1,2]. By 2021, the global market size reaches $3.78 billion, with a projected annual growth rate of 5.18% through 2030[3]. Deltamethrin (DLM), a high-efficacy synthetic pyrethroid insecticide, is extensively utilized in agricultural pest control[4,5]. However, with its steadily increasing application, environmental residues of DLM have raised global concern, with concentrations detected as high as 24–121 μg/L in agricultural and aquatic systems. Environmentally accumulated DLM enters organisms through the food chain or direct exposure. Studies have confirmed that high-dose DLM (e.g., 15–45 mg/kg in quails; 5–25 mg/kg in Swiss mice) induces acute toxicity in multiple organs including the heart, liver, brain and kidneys[6–9].

To investigate the chronic effects of long-term low-dose DLM exposure, we establish a female BALB/c mice model (DLM 0.2 mg/kg/day, oral gavage for 8 weeks; the dose is set according to Chinese food safety standards)[10], results indicate that chronic DLM exposure leads to significant DLM accumulation in intestinal tissues, accompanied by weight loss, increased disease activity index (DAI) scores and morphological changes such as reduced intestinal length[10–12]. Further molecular analyses reveal that intestinal mucosal barrier impairment is associated with redox homeostasis imbalance, cellular senescence and activation of apoptosis pathways[13–15]. Additionally, DLM exposure disrupts gut microbiota homeostasis, characterized by reduced microbial diversity, a decline in beneficial bacteria (e.g., *Lactobacillus*) and enrichment of potentially pathogenic genera (e.g., *Odoribacter* and *Bacteroides*)[16–18].

Cold atmospheric plasma (CAP), an ionized gas generated by electrical discharge[19,20], has garnered increasing research interest in biomedical and environmental sciences due to its ability to operate effectively at near-room temperature[21]. However, the limited tissue coverage and inconvenience of direct application have restricted its broader utility. To address these limitations, plasma-activated solutions (PAS), indirect CAP derivatives generated by plasma-treated liquids, have gained significant attention.

PAS retain the bioactive properties of CAP while offering enhanced applicability through liquid-phase delivery. PAS contain various reactive species including reactive oxygen and nitrogen species (ROS/RNS), short-lived radicals such as hydroxyl radicals (·OH), superoxide anions(O_2^-) and longer-lived molecules like ozone (O_3), nitric oxide (·NO), nitrogen dioxide ($\cdot NO_2$) and peroxynitrite ($ONOO^-$), which form a complex reactive system[22]. Studies indicate that PAS not only exhibit effective surface disinfection but also facilitate wound healing through regulating cell proliferation activity and mediating inflammatory responses[23,24]. In context of inflammatory bowel disease, therapeutic benefits mediated via ROS/RNS signaling pathways have been further validated[25,26].

Previous studies utilizing the Dextran Sulfate Sodium (DSS)-induced colitis model have demonstrated that PAS ameliorate colitis and reduce recurrence by promoting mucosal regeneration, alleviating inflammatory responses, rebalancing redox homeostasis and correcting gut microbial dysbiosis[10,13].

A critical challenge posed by pervasive DLM contamination is the absence of targeted therapies for chronic toxicity, a problem compounded by the suboptimal biocompatibility of existing antidotes. Our study aims to repurpose plasma-activated solutions, which are biocompatible, engineering-derived therapeutic agent to address this gap by developing PAS that couple high antagonistic efficacy with superior biocompatibility. To investigate whether PAS confer comparable reparative effects on intestinal mucosal barrier impairment induced by chronic low-dose DLM exposure, we propose a novel strategy to mitigate agricultural chemical-induced intestinal damage. To establish a female BALB/c mice model, we elucidate the nitrogen-dependent mechanistic basis of PAS to provide insights into detoxification pathways, paving the way for designing precision antidotes. The successful implementation of this research is anticipated to yield dual translational benefits: advancing clinical interventions for pesticide-related health risks and establishing a sustainable plasma-based platform for environmental health applications.

Results

PAS alleviated DLM-induced intestinal impairment

To investigate the therapeutic effects of PAS in mice chronically exposed to low-dose DLM, we set up four groups: the control group (Ctrl), the DLM-exposed group (DLM), the DLM + PAS treatment group (DLM + PAS) and the PAS-only group (PAS), DLM was administered by oral gavage for 8weeks (Fig. 1B). PAS were prepared by treating ddH_2O for 2 min at 3 cm below a plasma jet before free access to PAS (Fig. 1A)[21,27,28]. Compared to the DLM, PAS treatment restored body weight ($p < 0.001$), decreased DAI scores ($p < 0.001$) and attenuated the DLM-induced intestinal shortening ($p < 0.001$), proving PAS could heal pesticide-caused intestinal impairment (Fig. 1C-F).

H&E staining of intestinal tissues revealed normal morphology in the PAS comparable to the Ctrl group. DLM exposure induced intestinal epithelial inflammation with extensive inflammatory cell infiltration and architectural distortion of the intestinal mucosa including shortened villi and disrupted crypts ($p < 0.001$). PAS

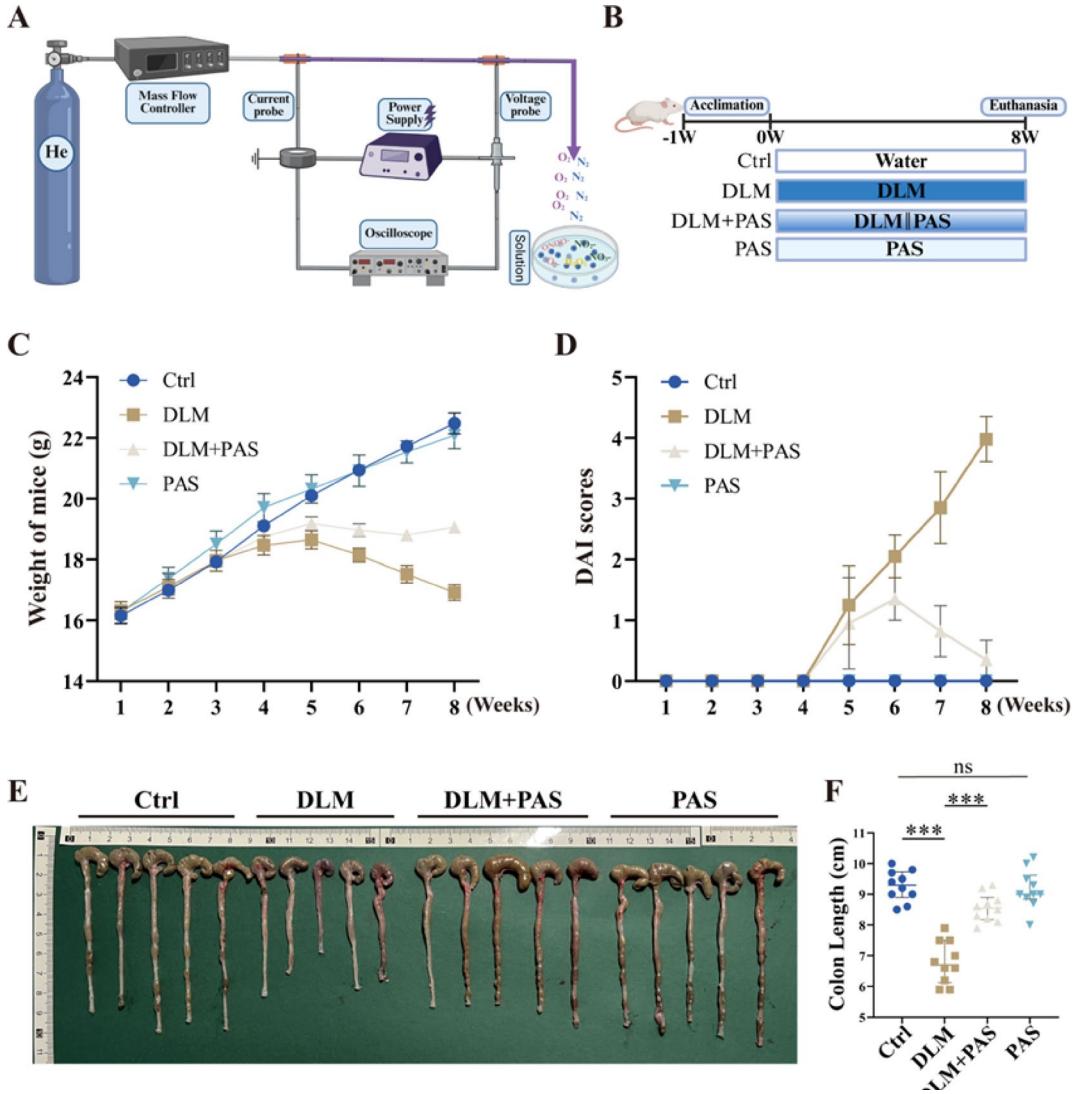

Fig. 1. PAS alleviated DLM-induced intestinal mucosal barrier impairment (**A**) Schematic diagram of PAS generation apparatus. (**B**) Schematic of PAS therapeutic intervention in chronic low-dose DLM-exposed murine models ($n = 10$). (**C**) PAS administration reversed DLM-induced body weight loss in mice ($n = 10$). (**D**) PAS intake reduced the elevated DAI scores induced by DLM ($n = 10$). (**E**,**F**) DLM exposure markedly reduces colon length, whereas PAS treatment significantly increase colon length compared to the DLM group. Administration of PAS alone have no effect on colon length relative to the control group ($n = 10$). Data were presented with mean ± SD. $^{*}p < 0.05$, $^{**}p < 0.01$, $^{***}p < 0.001$, ns: no significance.

co-treatment significantly reduced epithelial inflammation and infiltration, restoring tissue morphology to near-normal levels as evidenced by diminished inflammatory infiltration and restored mucosal architecture (Fig. 2A-B, $p < 0.05$). TUNEL staining further confirmed significantly decreased epithelial apoptosis in the DLM + PAS group versus the DLM group (Fig. 2C-D, $p < 0.001$), collectively indicating PAS-mediated mitigation of DLM-induced intestinal impairment. ELISA quantification of serum cytokines (IL-1β, IL-6, TNF-α) demonstrated significantly lower levels in the DLM + PAS versus DLM group (Fig. 2E-G, $p < 0.001$)[29,30]. Systemic H&E staining of organs from PAS-treated mice confirmed normal intestinal morphology, indicating high biocompatibility (Supplementary Fig. 1). These findings supported the potential therapeutic strategy of PAS for mitigating DLM-induced intestinal impairment[12,31,32].

PAS attenuated DLM-induced intestinal barrier impairment and redox homeostasis imbalance

Given prior evidence that chronic low-dose DLM exposure induced intestinal mucosal barrier impairment and redox homeostasis imbalance, we investigated whether PAS alleviated impairment through the same mechanisms[13]. TUNEL staining confirmed that PAS co-treatment reduced DLM-induced cell apoptosis (Fig. 2C-D). Immunofluorescence staining of apoptosis markers demonstrated that PAS decreased caspase-3 protein levels while upregulated Bcl-2 expression, further validating their anti-apoptotic effect (Fig. 3A-B). In vitro

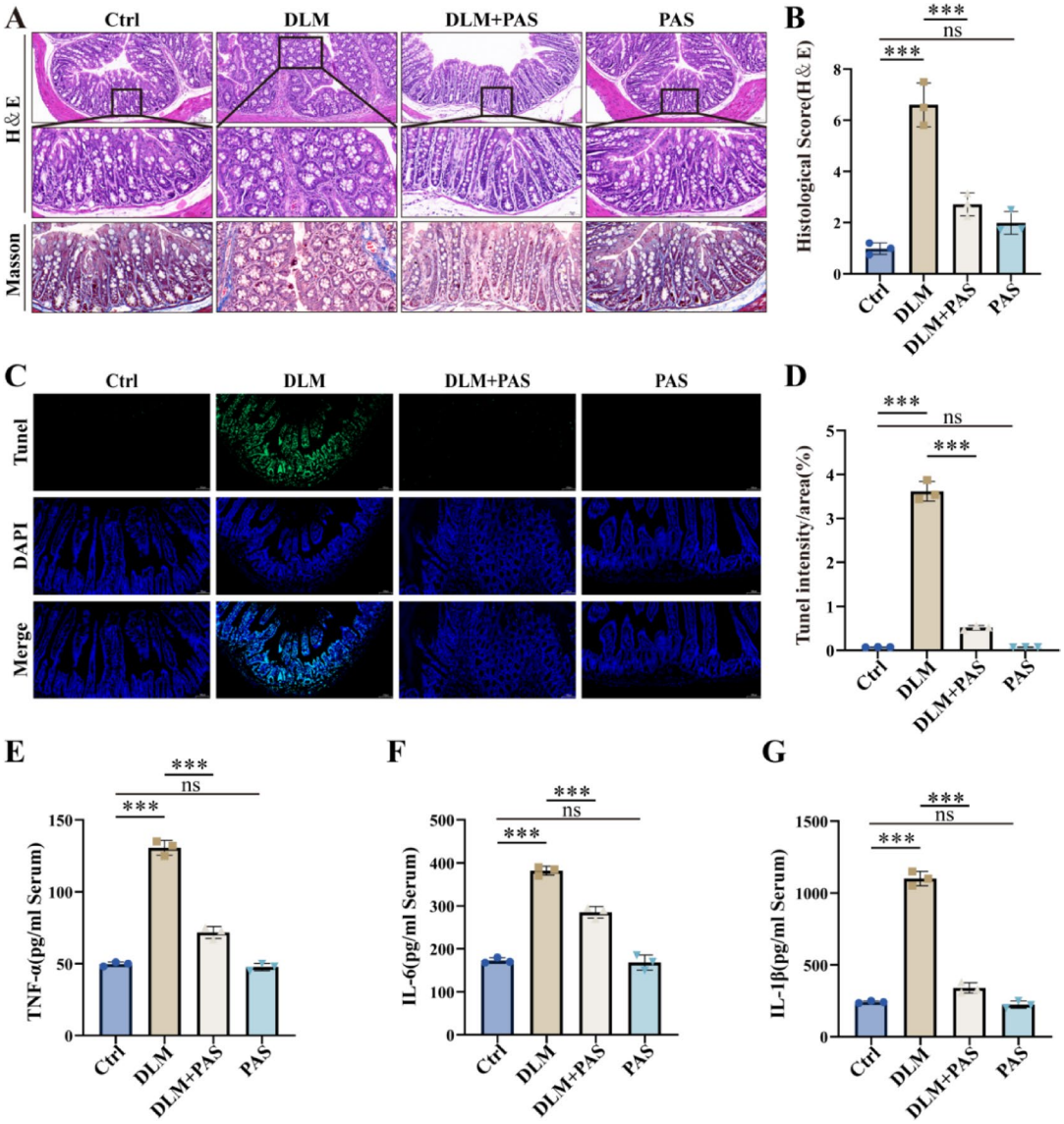

Fig. 2. PAS alleviated DLM-induced intestinal mucosal barrier impairment (**A**). The HE staining of intestinal tissue (20×; 40×) demonstrated PAS could clear DLM-induced intestinal mucosal barrier impairment ($n = 5$). Scale bars, 50 μm for 40×. (**B**) PAS treatment reduced intestinal mucosal barrier impairment caused by DLM in intestinal tissue ($n = 5$). (**C**,**D**) The Tunel staining of intestinal tissue (40×) confirmed that PAS reduced DLM-induced apoptosis in intestinal epithelial cells ($n = 5$). Scale bars, 50 μm for 40×. (**E**–**G**) ELISA quantification of inflammatory cytokines in murine serum revealed attenuated inflammation following PAS intervention in DLM-exposed models ($n = 3$). Data were presented with mean ± SD. *$p < 0.05$, ** $p < 0.01$, *** $p < 0.001$, n.s.: no significance.

validation using HCT-116 cells showed that PAS treatment reversed DLM-induced glutathione (GSH) depletion (Fig. 3D, $p < 0.001$)[33,34]. Representative immunofluorescence images revealed PAS significantly reduced DLM-triggered ROS accumulation in intestinal tissues (Fig. 3C, $p < 0.001$). Statistical analysis of these results was shown in Fig. 3E[35]. These results confirmed that PAS reduced DLM-induced cell apoptosis and redox imbalance, thereby protecting intestinal mucosal barrier function.

PAS mitigated DLM-induced cellular senescence

Previous studies demonstrated that although apoptosis levels decreased significantly after DLM discontinuation, barrier impairment symptoms persisted[10]. Further studies revealed that chronic low-dose DLM exposure induced cellular senescence in murine intestinal tissues[25]. This is the key factor impeding post-cessation recovery. To determine whether PAS ameliorated DLM-induced intestinal mucosal barrier impairment by counteracting cellular senescence, intestinal tissues were subjected to senescence-associated β-galactosidase (SA-β-gal) staining[36]. Results confirmed PAS significantly reduced DLM-triggered cellular senescence (Fig. 4A, $p < 0.001$).

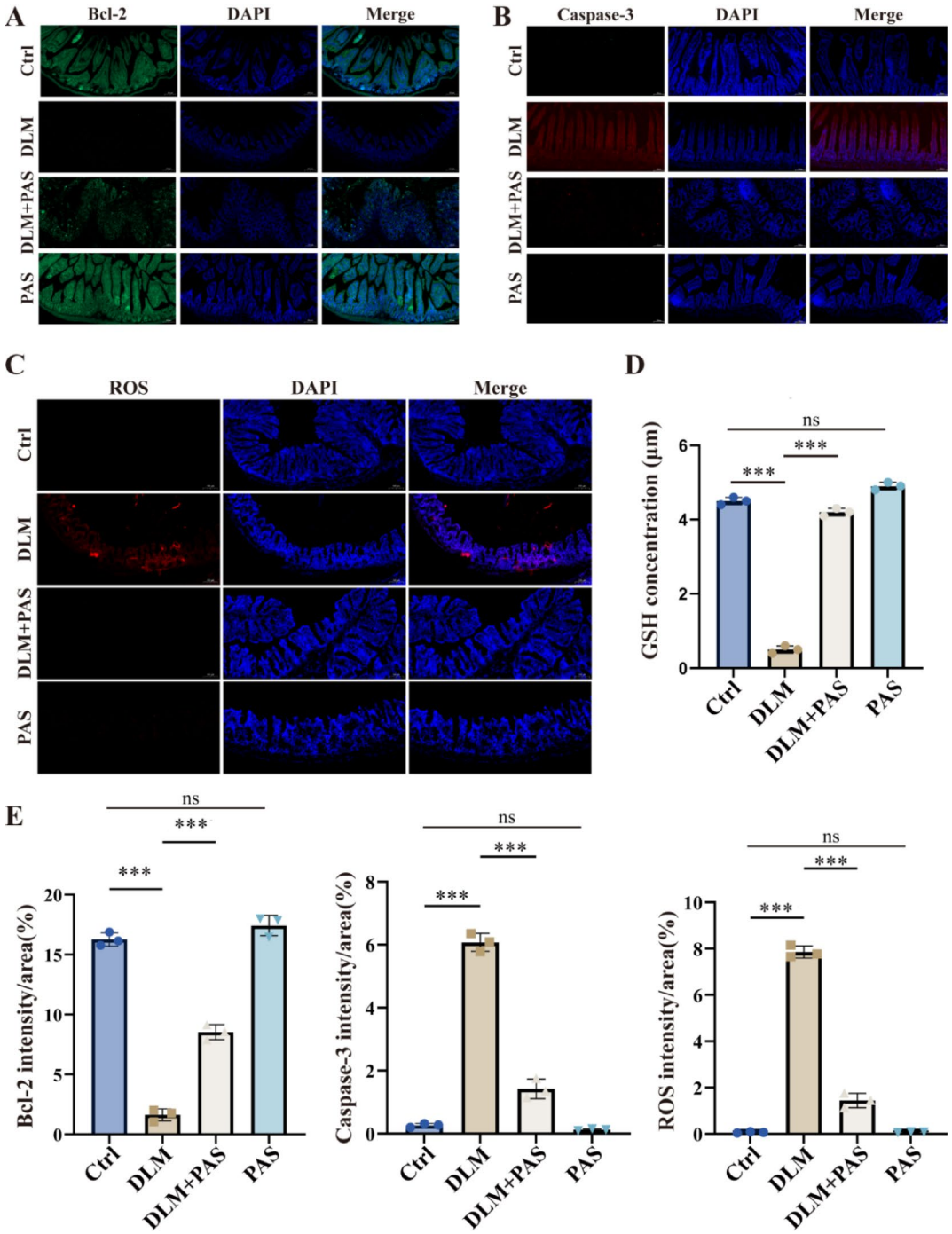

Fig. 3. PAS rebalanceed DLM-induced redox homeostasis (**A**,**B**). Immunofluorescence (IF) staining of intestinal tissue (40×) demonstrated that PAS treatment reversed DLM-induced upregulation of Caspase-3 and downregulation of Bcl-2 ($n = 3$). (**C**) Representative immunofluorescence images (40×) showing PAS ameliorated DLM-induced reactive oxygen species (ROS) accumulation in intestinal tissue ($n = 3$). Scale bars, 50 μm for 40×. (**D**) Altered GSH levels in HCT-116 cells after 48-hour DLM treatment. (**E**) Quantitative analysis of IF staining of A-C ($n = 3$). Data were presented with mean ± SD. *$p < 0.05$, ** $p < 0.01$, *** $p < 0.001$, n.s.: no significance.

Immunofluorescence staining revealed PAS downregulated senescence biomarkers P16 and P21 in DLM-exposed intestinal tissues (Fig. 4B-C, Figure S2A-B). Furthermore, immunofluorescence also demonstrated PAS suppressed DLM-induced activation of the P53 signaling pathway, which is the critical mediator of senescence associated mechanisms (Fig. 4D, Figure S2C).

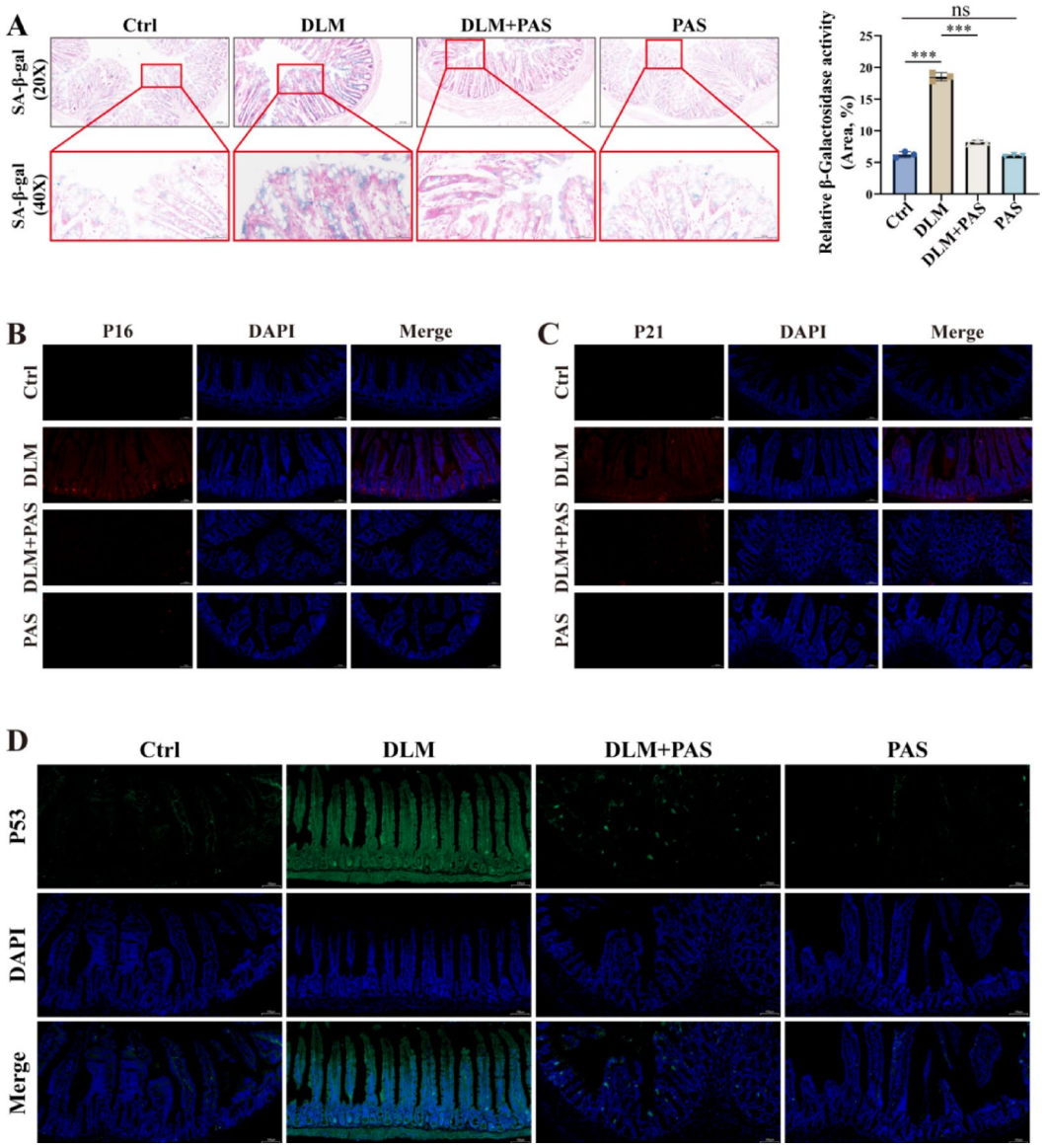

Fig. 4. PAS mitigated DLM-induced cellular senescence (**A**) SA-β-gal staining (20×; 40×) demonstrated PAS reversed cellular senescence in intestinal tissue induced by chronic DLM exposure ($n = 3$). Scale bars, 50 μm for 40× (**B**,**C**) Immunofluorescence (IF) staining (40×) demonstrated that PAS intake downregulated elevated p21 and p16 expression in DLM-exposed intestinal tissue ($n = 3$). Scale bars, 50 μm for 40×. (**D**) Immunofluorescence (IF) staining (40×) of intestinal tissue demonstrated that PAS treatment blocked the p53 signaling pathway activated in intestinal epithelial cells by chronic DLM exposure ($n = 3$). Scale bars, 50 μm for 40×. Data were presented with mean ± SD. *$p < 0.05$, ** $p < 0.01$, *** $p < 0.001$, n.s.: no significance.

The therapeutic effects of PAS primarily depend on reactive nitrogen species

PAS constituted a mixture of ROS/RNS that ultimately decomposed into hydrogen peroxide and nitrate/nitrite[21]. Existing evidence indicated that exogenous nitrate ameliorated DSS-induced intestinal mucosal barrier impairment. To explore RNS as primary therapeutic mediators, we developed nitrogen-depleted PAS (Nitro-Free PAS)[28]. To validate the therapeutic effects of Nitro-Free PAS on DLM-induced intestinal impairment, we employed three groups: the DLM group, the DLM + PAS treatment group and the DLM + PAS-Nitro-Free treatment group (Fig. 5A). Compared to the 2-minute PAS, extending the treatment time to 5 min did not increase the nitrate/nitrite concentration in ddH_2O. Therefore, 2-minute Nitro-Free PAS were prepared and subsequent ion chromatography analysis confirmed a significant reduction in nitrate/nitrite content (Fig. 5F-G, $p < 0.001$).

After an 8-week intervention, the therapeutic effects were markedly attenuated in the DLM + Nitro-Free PAS group. Intestinal lengths remained comparable to DLM-exposed mice and failed to recover to normal length (Fig. 5D-E). Simultaneously, the DLM + Nitro-Free group exhibited reduced body weight and increased DAI scores, showing no significant difference compared to the DLM group (Fig. 5B-C, Figure S3A-B). These

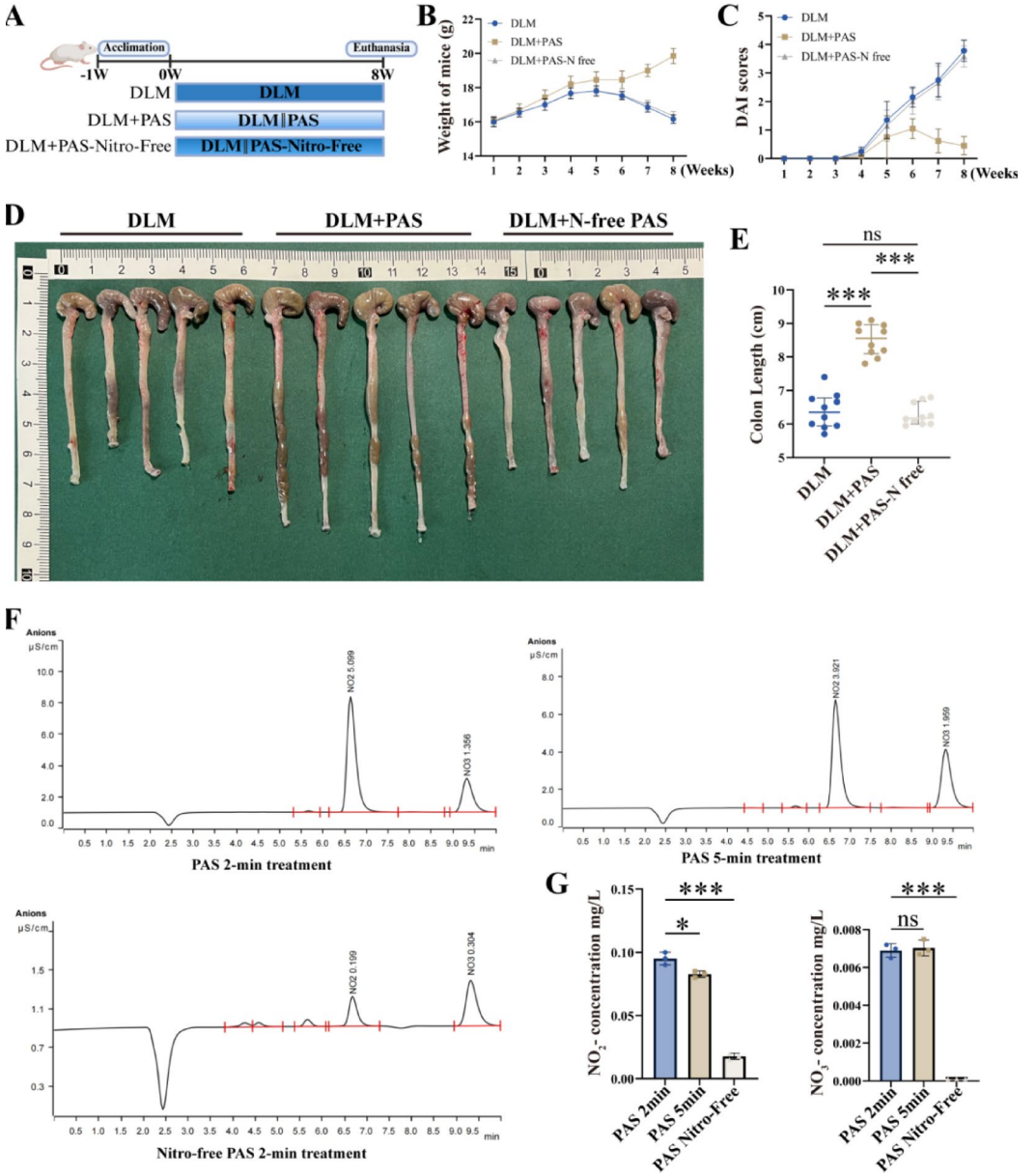

Fig. 5. The therapeutic effects of PAS primarily depend on reactive nitrogen species (**A**) Diagram showing PAS treatment in animals with long-term low-dose DLM exposure ($n = 10$). (**B**) Nitro-Free PAS failed to reverse DLM-induced body weight loss in mice ($n = 10$). (**C**) Nitro-Free PAS failed to reduce elevated DAI scores caused by DLM exposure ($n = 10$). (**D**, **E**) After Nitro-Free PAS intake, DLM-induced intestinal shortening failed to be restored ($n = 10$). (**F**,**G**) Compared to the 2-minute treatment, the 5-minute treatment did not increase nitrate/nitrite levels. Ion chromatography confirmed substantially diminished or abolished nitrate/nitrite levels in ddH_2O treated with the nitrogen-depleted generator, validating the efficacy of nitrogen oxide-depleted PAS. Data were presented with mean ± SD. *$p < 0.05$, ** $p < 0.01$, *** $p < 0.001$, n.s.: no significance.

preliminary findings indicated that nitrogenous components were the primary determinant of PAS-mediated therapeutic effects against DLM-induced intestinal mucosal barrier impairment.

PAS rebalanced redox homeostasis and attenuated cellular senescence via RNS-dependent manner

To further validate this conclusion, histological analysis of intestinal tissues from all three groups was performed. H&E staining revealed persistent inflammation and barrier impairment following Nitro-free PAS treatment (Fig. 6A, $p < 0.001$), while TUNEL staining indicated increased apoptosis compared to PAS intervention (Fig. 6B, E, $p < 0.001$). To determine whether PAS exerted therapeutic effects through RNS-mediated modulation of redox homeostasis imbalance and cellular senescence, the levels of caspase-3 in intestinal tissues were determined by immunofluorescence staining and ROS accumulation was evaluated using fluorescent staining. Nitro-free PAS

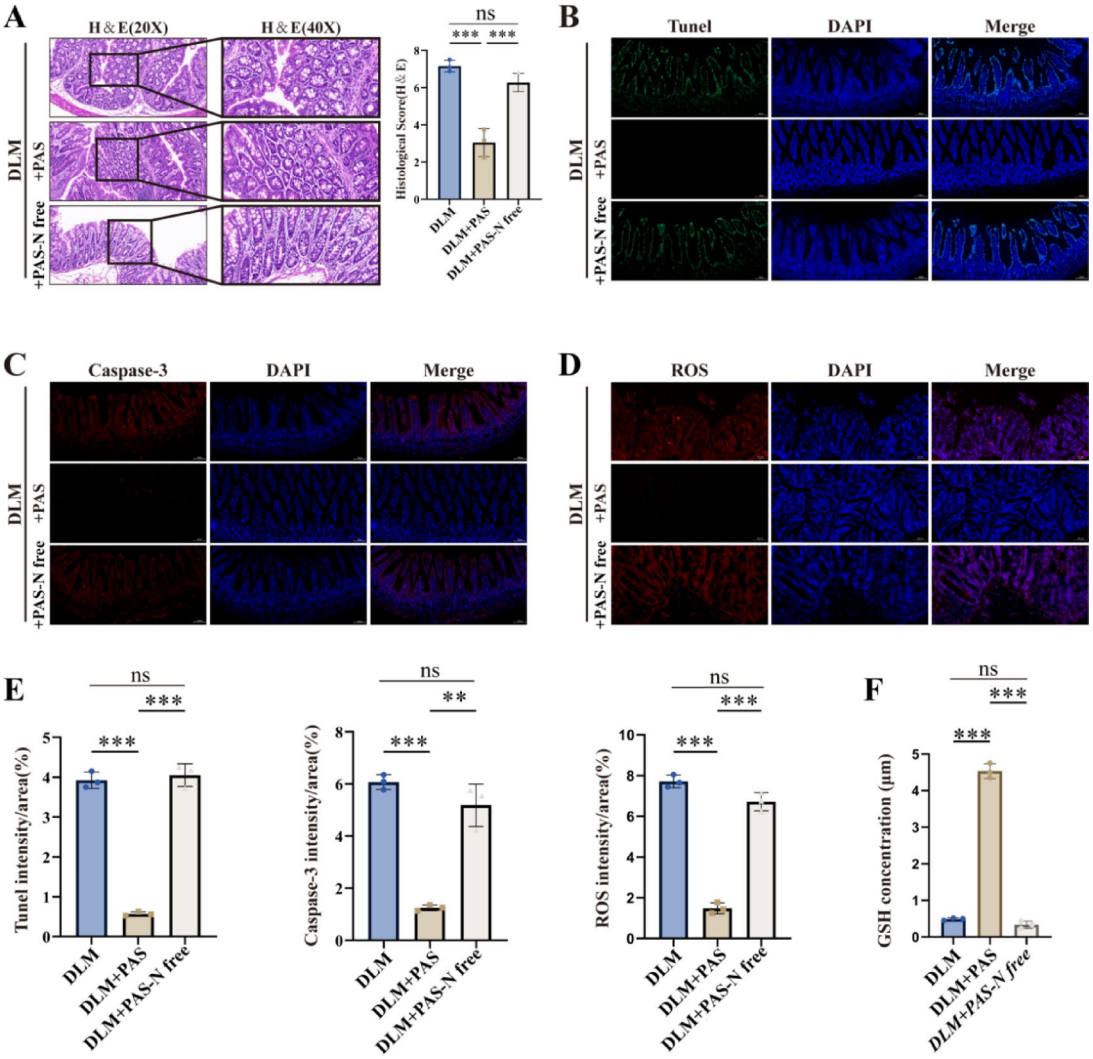

Fig. 6. PAS rebalanced redox homeostasis via RNS-dependent manner (**A**). The H&E staining of intestinal tissue (20×; 40×) demonstrated PAS alleviated inflammatory cell infiltration via RNS-dependent manner ($n = 3$). Scale bars, 50 μm for 40×. (**B**) The Tunel staining of intestinal tissue (40×) confirmed PAS reduced DLM-induced apoptosis via RNS-dependent manner ($n = 3$). Scale bars, 50 μm for 40×. (**C**) Immunofluorescence (IF) staining of intestinal tissue (40×) demonstrated that PAS treatment reversed DLM-induced upregulation of Caspase-3 via RNS-dependent manner ($n = 3$). Scale bars, 50 μm for 40×. (**D**) Representative immunofluorescence images (40×) showing PAS ameliorated DLM-induced ROS accumulation in intestinal tissues via RNS-dependent manner ($n = 3$). Scale bars, 50 μm for 40×. (**E**) Quantitative analysis of IF staining of A-C ($n = 3$). (F) Altered GSH levels in HCT-116 cells after 48-hour DLM treatment. Data were presented with mean ± SD. *$p < 0.05$, ** $p < 0.01$, *** $p < 0.001$, n.s.: no significance.

failed to suppress DLM-induced ROS elevation in intestinal tissues and did not reduce caspase-3 expression (Fig. 6C-D, E, $p < 0.001$). Concurrently, oxidative stress assays demonstrated that Nitro-free PAS could not reverse DLM-triggered GSH depletion in HCT-116 cells (Fig. 6F, $p < 0.001$).

SA-β-gal staining showed nitro-free PAS failed to mitigate DLM-induced cellular senescence (Fig. 7A,B, $p < 0.001$). Immunofluorescence staining further confirmed that Nitro-free PAS did not downregulate DLM-elevated senescence biomarkers (P16, P21) (Fig. 7C-D). This effect was achieved through coordinated mechanisms: suppressing epithelial apoptosis, modulating redox homeostasis, counteracting cellular senescence and ultimately treating DLM-induced intestinal mucosal barrier impairment (Fig. 8).

Discussion

As a widely employed agricultural insecticide, DLM progressively accumulates in the environment and enters the human body through multiple pathways contributing multi-organ toxicity. Our prior in vivo and in vitro studies demonstrate that chronic low-dose DLM exposure induced intestinal mucosal barrier impairment via promotion of epithelial apoptosis, disruption of redox homeostasis and induction of cellular senescence

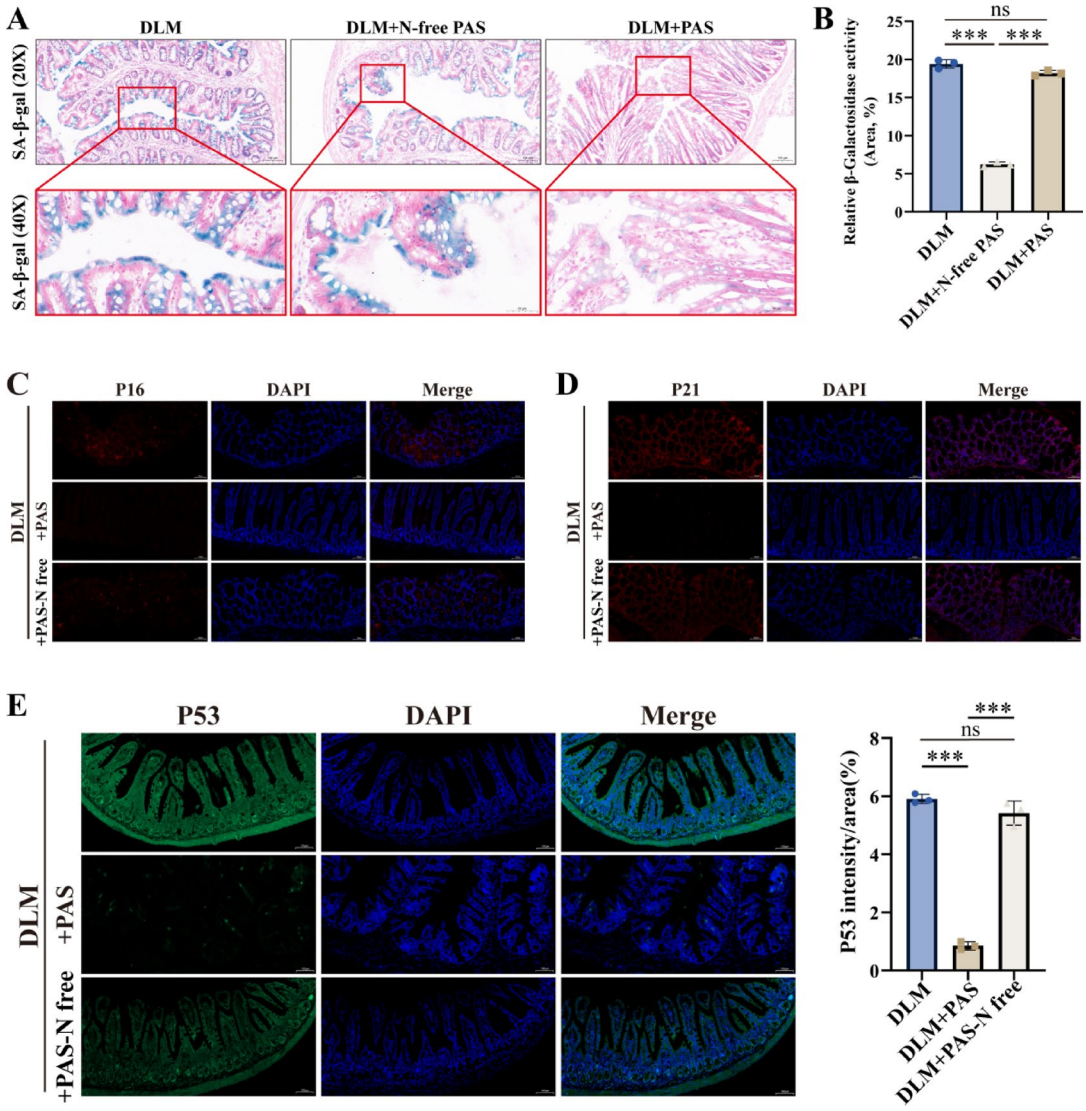

Fig. 7. PAS attenuated cellular senescence via RNS-dependent manner (**A**,**B**). SA-β-gal staining (20×; 40×) demonstrated PAS reversed cellular senescence in intestinal tissue induced by chronic DLM exposure via RNS-dependent manner ($n = 3$). Scale bars, 50 μm for 40×. (**C**,**D**) Immunofluorescence (IF) staining (40×) demonstrated that PAS intake downregulated elevated p21 and p16 expression in DLM-exposed intestinal tissue via RNS-dependent manner ($n = 3$). Scale bars, 50 μm for 40×. (**E**) Immunofluorescence (IF) staining of intestinal tissues (40×) demonstrated that PAS treatment blocked the p53 signaling pathway activated in intestinal epithelial cells by chronic DLM exposure via RNS-dependent manner ($n = 3$). Scale bars, 50 μm for 40×. Data were presented with mean ± SD. $^{*}p < 0.05$, $^{**}p < 0.01$, $^{***}p < 0.001$, n.s.: no significance.

leading to cell cycle arrest[10,13]. Given these multi-organ adverse effects, developing effective and biocompatible therapeutic strategies is imperative.

PAS, which are indirect derivatives of cold atmospheric plasma generated by treating ddH_2O with plasma, have attracted considerable interest. PAS contain high-energy particles such as ROS and RNS, alongside short-lived and persistent reactive components[37–39]. Our preliminary studies reveal therapeutic efficacy of PAS in inflammatory bowel diseases through mucosal healing, inflammation mitigation and restoration of redox homeostasis[21]. Based on these findings, we propose that PAS can similarly ameliorate DLM-induced intestinal mucosal barrier impairment. Consequently, experiments are performed to validate this hypothesis and elucidate the underlying mechanisms.

Initially, a BALB/c female mice model of DLM-induced intestinal mucosal barrier impairment is established, with the treatment group receiving free access to PAS[40,41]. Therapeutic intervention demonstrates that PAS significantly ameliorate DLM-induced intestinal impairment, evidenced by restored body weight, lowered DAI scores and improved intestinal length. Concurrently, H&E staining reveals PAS mitigate inflammatory cell infiltration and preserve intestinal epithelial integrity.

To further validate the mechanistic basis, further histological analyses are conducted. PAS administration reduce TUNEL-positive cell areas and modulate apoptosis regulators, concurrently restoring GSH homeostasis

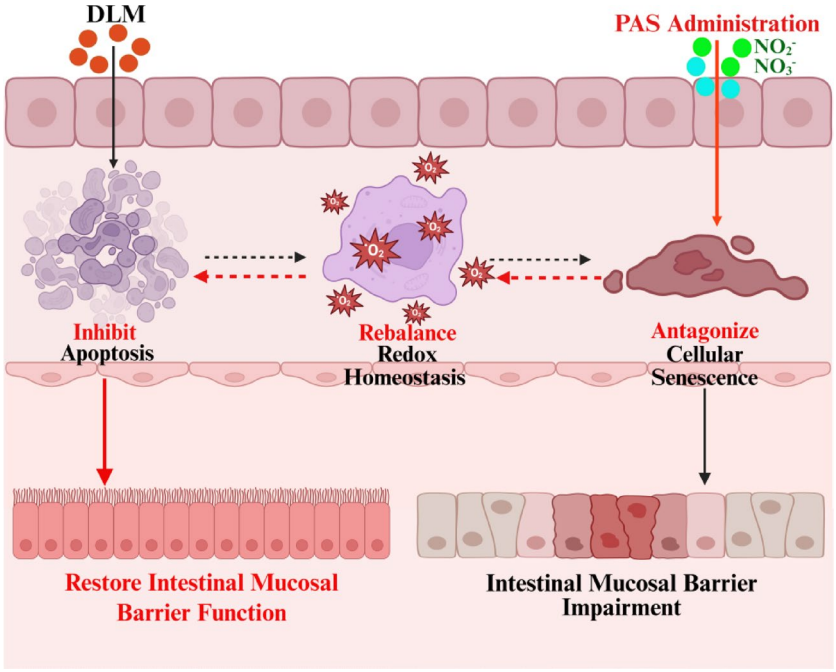

Fig. 8. Mechanism diagram illustrating the role of PAS in DLM-induced intestinal mucosal barrier injury.

and decreasing ROS accumulation, indicating redox homeostasis protection. Additionally, PAS diminish SA-β-gal-positive cells, downregulate senescence biomarkers, suppress p53 signaling, effectively counteract cellular senescence and alleviate cell cycle arrest. These results collectively validate our initial hypothesis, PAS alleviate DLM-triggered intestinal mucosal barrier impairment through inhibiting apoptosis, rebalancing redox homeostasis and counteracting cellular senescence.

Given the therapeutic effects of PAS on chronic low-dose DLM-induced intestinal mucosal barrier impairment, we investigate their active components. Reviews indicate CAP contains diverse reactive species including ROS, RNS and energetic particles-ranging from short-lived components like hydroxyl radicals (·OH), superoxide (O_2^-) and ozone (O_3) to stable molecules such as nitric oxide (NO), nitrogen dioxide (·NO_2) and peroxynitrite ($ONOO^-$)[42,43]. Prior studies using DSS-colitis models establish nitrogenous compounds as primary mediators in PAS-mediated colitis treatment, prompting our hypothesis that these components similarly drive PAS efficacy against DLM-induced barrier impairment[40,44]. To validate this, nitrogen oxide-free PAS are assessed in our chronic low-dose DLM model, after 8-week intervention, therapeutic efficacy is markedly attenuated or abolished, histological analyses confirm that compared to the PAS group, apoptosis increased (indicated by increased TUNEL-positive cells), ROS accumulation enhanced and cellular senescence exacerbated. These findings definitively establish nitrogenous components as indispensable mediators underpinning PAS-conferred protection against DLM-induced intestinal injury.

Although our preliminary findings confirm that PAS promote restoration of intestinal mucosal barrier function by regulating redox homeostasis through RNS release, existing nitrogen-free PAS generators still cannot fully eliminate RNS. Therefore, the reliability of these conclusions requires further refinement of experimental apparatus and replicated validation. Concurrently, comprehensive clinical data collection must be expedited to translate PAS into preliminary clinical applications, which will further substantiate their clinical efficacy.

Our previous studies reveal that DLM-induced barrier impairment disrupts gut microbiota homeostasis[45–47]. Parallel research in DSS-induced colitis models demonstrate that PAS intervention effectively suppresses inflammation, enhances intestinal mucosal barrier function and partially restores microbial diversity[48]. Whether PAS confer similar restorative effects on DLM-disrupted gut microbiota remains unknown. Subsequent investigations will focus on elucidating PAS-induced alterations in gut microbiota following barrier impairment, thereby exploring deeper mechanistic insights into PAS-mediated intestinal protection.

Our results demonstrate that PAS significantly alleviate DLM-induced intestinal mucosal barrier injury. Although our study primarily documents phenotypic recovery including reducing apoptosis, cellular senescence and inflammatory response, the underlying molecular mechanisms warrant further clarification. The therapeutic efficacy of PAS is likely mediated by its diverse reactive species, particularly RNS including nitric oxide and nitrogen dioxide, which is a key signaling molecule involved in multiple biological processes. For example, studies on PAS in wound management have indicated that it modulates the PI3K/Akt pathway[39], a critical regulator of cell survival and apoptosis. It is plausible that in our model, PAS-derived NO activate similar pro-survival signaling, thereby counteracting DLM-induced epithelial apoptosis. Furthermore, the observed attenuation of oxidative stress may be associated with the activation of the Nrf2 pathway[49], a master regulator of antioxidant response, which can be triggered by RONS present in PAS. The reduction in cellular senescence may also be attributed to the modulation of p53/p21 and p16 pathways[50], which are centrally involved in the regulation of

senescence. Thus, we propose that PAS orchestrate a multi-faceted response targeting apoptosis, oxidative stress and cellular senescence through their nitrogen-based components. Further investigations focusing on these specific pathways will be essential to validate the proposed mechanisms.

In summary, this study confirms PAS as a potent therapeutic agent against chronic DLM-induced intestinal mucosal barrier impairment, operating through suppressing apoptosis, preserving redox homeostasis, counteracting cellular senescence and alleviating cell cycle arrest. Nitrogenous compounds derived from PAS serve as the primary therapeutic mediators. Comprehensive histopathological assessment demonstrates favorable biocompatibility of PAS, supporting their potential application as an effective countermeasure against DLM-induced human health risks.

Conclusion

This study confirms that PAS administered via drinking effectively reverse chronic low-dose DLM-induced intestinal mucosal barrier impairment. The reparative mechanism involves restoring redox homeostasis, thereby inhibiting cellular senescence and restoring cell cycle progression. To identify the active components, nitro-free PAS are tested. Results demonstrate that after 8 weeks of Nitro-free PAS intervention, no or minimal therapeutic efficacy is observed against intestinal mucosal barrier impairment. This identifies RNS as the core mediator underpinning PAS-conferred protection, operating through redox balance regulation and anti-senescence pathways. These findings provide a novel strategy for pesticide toxicity intervention, applicable not only to DLM and other pyrethroids but also with potential broader-spectrum utility against diverse pesticide exposures.

Materials and methods

Production of Plasma-activated solutions and Nitro-free PAS

Figure 1A shows the atmospheric plasma generation system. Plasma is produced in a helium dominant atmosphere using an input voltage of 12.4 kV and gas flow at 15 L/min. We place 6 mL ddH_2O 3 cm below the plasma jet for 2-minute and 5-minute treatment before ion chromatographic analysis. Results indicate that extending the treatment duration to 5 min did not increase the nitrate/nitrite concentration in PAS. Therefore, PAS prepared with a 2-minute treatment is selected for subsequent investigations. To prepare Nitro-free PAS, we reconfigure the plasma device to establish a helium saturated environment during operation. Post-CAP treatment RONS concentrations in the medium are measured via ion chromatography.

Animal experiment

BALB/c female mice (4-week old, weighted about 16 g) are sourced from the Laboratory Animal Center, Xi'an Jiaotong University Health Science Center (Xi'an, China). All animal procedures comply with institutional ethical guidelines and receive approval from Xi'an Jiaotong University's Animal Ethics Committee (Approval ID: 2024 – 1803).To investigate the therapeutic effects of PAS in mice chronically exposed to low-dose DLM, forty 4-week-old female BALB/c mice (body weight approximately 16 g) are randomly divided into four groups: (1) Control group (free access to ddH_2O, 8 weeks); (2) DLM group (DLM, oral gavage, 0.2 mg/kg/day, 8 weeks); (3) DLM + PAS group (DLM, 0.2 mg/kg/day, 8 weeks; free access to PAS, 8 weeks. PAS were refreshed daily to maintain activity); (4) PAS-alone group (free access to PAS, 8 weeks), with 10 mice per group. To study how PAS work therapeutically, thirty 4-week-old female BALB/c mice (body weight approximately 16 g) are randomly divided into three groups: (1) DLM group (DLM, oral gavage, 0.2 mg/kg/day, 8 weeks); (2) PAS group (free access to PAS, 8 weeks); (3) PAS-Nitro-free group (free access to N-free PAS, 8 weeks) with 10 mice per group. All mice are raised in a specific pathogen-free (SPF) environment with controlled temperature (22 ± 2 °C) and a 12-hour light/dark cycle. Body weight is measured weekly and DAI scores are assessed throughout the experiment. After eight weeks of intervention, tail vein phlebotomy under anesthesia, feces are collected followed by euthanasia. Anesthesia is induced with sodium pentobarbital (40 mg/kg, i.p.), followed by euthanasia via supplemental pentobarbital administration (160 mg/kg, i.p.) to achieve a terminal dose of 200 mg/kg, with death confirmed by thoracotomy. Intestinal tissues are dissected, intestinal length is measured and tissues are collected for subsequent histological analysis. Alignment with ARRIVE Essentials: (1) The individual mouse was defined as the experimental unit for all analyses. (2) Group assignment used a computer-generated random number sequence, with allocation concealed by sealing codes in opaque envelopes until intervention began. (3) Outcome assessments (H&E/TUNEL/IF quantification, DAI scores) were performed by investigators blinded to group assignments. (4) Healthy female BALB/c mice (12 weeks old) were included; animals exhibiting signs of systemic illness or technical errors (e.g., tissue damage during processing) were excluded pre-analysis. (5) The sample size ($n = 10$) was determined based on our pilot data and previous studies using similar DLM exposure models. (6) No data points were excluded post-hoc. (7) All data are now presented as mean ± SD for each endpoint.

Cell line

The human colon cancer cell line HCT-116 (Procell) was cultured in PAS treated Dulbecco's Modified Eagle Medium (DMEM; Corning, 10-013-CVR) supplemented with 10% fetal bovine serum (FBS; Invitrogen, 16000-044) at 37 °C under a 5% CO_2 atmosphere, with medium replenishment every 2–3 days. This cell line was routinely tested for STR identity and mycoplasma contamination.

Hematoxylin-eosin (H&E) staining

Intestinal specimens are harvested following euthanasia procedures. Tissues undergo fixation in 4% paraformaldehyde solution. Subsequent to paraffin embedding, cryosectioning yielded 4–5 μm thick slices for hematoxylin-eosin (H&E) staining. H&E-stained histopathological injuries were independently evaluated by two pathologists blinded to the experimental groups.

Immunofluorescence analysis

For immunofluorescence labeling, intestinal sections are subjected to primary antibody incubation for 120 min at 37 °C using the following reagents: caspase-3 antibody (Proteintech 19677-1-AP, 1:500), Bcl-2 antibody (Proteintech 26593-1-AP, 1:300), P16 antibody(Proteintech 28416-1-AP, 1:200), P21 antibody (Proteintech 28248-1-AP, 1:200) and p53 antibody (Proteintech 10442-1-AP, 1:200). After triple-washing with phosphate-buffered saline (PBS), sections received green Alexa Fluor® 568-conjugated secondary antibody (Proteintech rb2AF568, 1:500) for 60 min at 37 °C. Nuclear counterstaining employ 4′,6-diamidino-2-phenylindole (DAPI) (Beyotime C1002, 0.5 μg/mL). Fluorescence microscopy imaging is performed using a ZEISS Axio Observer 7 system (Germany).

Enzyme-linked immunosorbent assay

Following the 8-week experimental period, anesthetized mice underwent tail vein blood collection. Anesthesia was induced by intraperitoneal injection of sodium pentobarbital (40 mg/kg). Harvested whole blood samples were allowed to clot for 30 min at room temperature prior to centrifugation at 1000× g for 15 min. The resultant serum supernatant was transferred into 1.5 mL microcentrifuge tubes and cryopreserved at -20 °C. Before analysis, frozen serum specimens were equilibrated to ambient temperature. The assay procedure initiated with coating 96-well plates using capture antibodies; followed by concurrent incubation of serum samples with horseradish peroxidase–conjugated detection antibodies; proceeded through enzymatic development of chromogenic substrates; and concluded with microplate spectrophotometric quantification of target protein concentrations at manufacturer-specified wavelengths.

Terminal Deoxynucleotidyl transferase dUTP Nick-End labeling staining

Intestinal tissue apoptosis assessment was conducted using a commercial TUNEL detection system (Roche 11684817910). Following 5% paraformaldehyde fixation, specimens underwent paraffin embedding and sectioning at 4–5 μm thickness. Sequential dewaxing and hydration via ethanol gradient preceded proteolytic treatment with proteinase K solution (20 μg/mL, 15-minute incubation). After phosphate-buffered saline (PBS) rinsing, sections received blocking buffer (3% bovine serum albumin in PBS, 60 min). The TUNEL reaction mixture was subsequently applied for room temperature incubation (25 ± 2 °C, 60 min). Post-PBS washing, nuclear visualization employed 4′,6-diamidino-2-phenylindole (DAPI) counterstaining. Following triple PBS washing, apoptotic cells exhibiting green fluorescence (490–525 nm emission) were examined using a ZEISS Axio Observer 7 fluorescence imaging system.

Glutathione detection

After subjecting cells to 48-hour treatments with 50 μm DLM, PAS, or DLM + PAS, cellular material was harvested for glutathione (GSH) measurement employing a commercial detection system (Beyotime S0052) under manufacturer-prescribed conditions. GSH concentrations were spectrophotometrically determined at 421 nm wavelength using a BioTek Cytation 5 M multi-mode microplate reader, with absorbance values converted to quantitative measurements through standardized calibration protocols.

ROS detection

Cryopreserved tissue specimens (-80 °C storage) were immersed in Optimal Cutting Temperature compound (Sakura Tissue-Tek, 4583) for cryosectioning at 10 μm thickness using a cryostat, with sections adhered to glass slides. These frozen sections were maintained at -20 °C until analysis. Following standard protocols, dihydroethidium (DHE) fluorescent probe (Beyotime S0063) was employed for ROS detection. Summarily, sections were equilibrated to room temperature for 30 min after removal from − 20 °C storage. Subsequent distilled water washing cycles (8 min × 2) preceded fixation with 4% paraformaldehyde (15 min). Sections then received 10 μM DHE solution in phosphate-buffered saline (PBS) during 30-minute incubation at 37 °C within a humidified dark chamber; parallel negative controls used probe-free PBS. Excess fluorophore was eliminated through triple PBS washes (5 min each). Nuclear counterstaining utilized DAPI (10 min, ambient temperature) before anti-fade mounting. Immunofluorescent signals were captured using a Cytation5M imaging system (BioTek, USA) with 535 nm excitation/610 nm emission parameters. Quantitative analysis of fluorescence intensity employed Fiji software, with mean fluorescence intensity (MFI) values calculated from region-specific measurements.

Senescence-associated β-galactosidase (SA-β-Gal) staining

Given the established activation of SA-β-Gal activity during cellular senescence, Intestinal tissue sections were processed using a commercial detection kit (Beyotime C0602) to quantify senescent cell populations. Briefly, collected murine intestinal specimens were cryosectioned and fixed at ambient temperature for 30 min in kit-provided fixative/dye mixture. Following fixation, sections underwent three phosphate-buffered saline (PBS) washing cycles prior to overnight incubation (37 °C) with 30 μL staining solution that completely covered the sections. After removing unbound dye through triple PBS washes, tissue sections were mounted with anti-fade solution and examined under a phase-contrast light microscope. Senescent cells exhibited definitive blue chromogenic staining, with quantitative image analysis performed per standardized protocols.

Statistical analysis

Quantitative analyses employed GraphPad Prism v9.0 software (IBM Corporation), with datasets presented as mean ± standard deviation or proportional percentages. Intergroup comparisons utilized Student's t-test for continuous variables, chi-square test for categorical data, or one-way repeated-measures ANOVA where appropriate. Statistical significance threshold was established at $p < 0.05$ for all inferential tests, with post-hoc

Bonferroni adjustments applied during multiple comparisons. Statistical analyses were performed after verifying that all datasets satisfied the assumptions of homogeneity of variance and normality.

Data availability

The datasets generated during this study are available from the corresponding author on reasonable request, subject to institutional approval.

Received: 9 September 2025; Accepted: 10 December 2025
Published online: 21 January 2026

References

1. Deng, F. et al. Contamination of pyrethroids in agricultural soils from the Yangtze river Delta, China. *Sci. Total Environ.* **731**, 139181. https://doi.org/10.1016/j.scitotenv.2020.139181 (2020).
2. Basu, S., Chanda, A., Gogoi, P. & Bhattacharyya, S. Organochlorine pesticides and heavy metals in the zooplankton, fishes, and shrimps of tropical shallow tidal creeks and the associated human health risk. *Mar. Pollut Bull.* **165**, 112170. https://doi.org/10.1016/j.marpolbul.2021.112170 (2021).
3. Zhu, Q. et al. Photodegradation kinetics, mechanism and aquatic toxicity of deltamethrin, permethrin and dihaloacetylated heterocyclic pyrethroids. *Sci. Total Environ.* **749**, 142106. https://doi.org/10.1016/j.scitotenv.2020.142106 (2020).
4. Mestres, R. & Mestres, G. Deltamethrin: uses and environmental safety. *Rev. Environ. Contam. Toxicol.* **124**, 1–18. https://doi.org/10.1007/978-1-4612-2864-6_1 (1992).
5. Song, Y., Kai, J., Song, X., Zhang, W. & Li, L. Long-term toxic effects of deltamethrin and Fenvalerante in soil. *J. Hazard. Mater.* **289**, 158–164. https://doi.org/10.1016/j.jhazmat.2015.02.057 (2015).
6. Deng, N. et al. Inhibition of the Nrf2/p38MAPK pathway involved in deltamethrin-induced apoptosis and fibrosis in quail kidney. *Food Chem. Toxicol.* **155**, 112382. https://doi.org/10.1016/j.fct.2021.112382 (2021).
7. Han, B. et al. Deltamethrin induces liver fibrosis in quails via activation of the TGF-β1/Smad signaling pathway. *Environ. Pollut.*. **259**, 113870. https://doi.org/10.1016/j.envpol.2019.113870 (2020).
8. Hazarika, H. et al. Bioaccumulation of deltamethrin and piperonyl butoxide in Labeo Rohita fish. *Ecotoxicol. Environ. Saf.* **284**, 116908. https://doi.org/10.1016/j.ecoenv.2024.116908 (2024).
9. Lukowicz-Ratajczak, J. & Krechniak, J. Effects of deltamethrin on the immune system in mice. *Environ. Res.* **59**, 467–475. https://doi.org/10.1016/s0013-9351(05)80049-0 (1992).
10. Ma, R. et al. Chronic low-dose deltamethrin exposure induces colon injury and aggravates DSS-induced colitis via promoting cellular senescence. *Ecotoxicol. Environ. Saf.* **274**, 116214. https://doi.org/10.1016/j.ecoenv.2024.116214 (2024).
11. Wang, H. et al. Ginkgo Biloba extract alleviates deltamethrin-induced testicular injury by upregulating SKP2 and inhibiting Beclin1-independent autophagy. *Phytomedicine* **135**, 156245. https://doi.org/10.1016/j.phymed.2024.156245 (2024).
12. Li, J. et al. Toxicological effects of deltamethrin on quail cerebrum: weakened antioxidant defense and enhanced apoptosis. *Environ. Pollut.* **286**, 117319. https://doi.org/10.1016/j.envpol.2021.117319 (2021).
13. Ma, R. et al. Chronic exposure to low-dose deltamethrin can lead to colon tissue injury through PRDX1 inactivation-induced mitochondrial oxidative stress injury and gut microbial dysbiosis. *Ecotoxicol. Environ. Saf.* **264**, 115475. https://doi.org/10.1016/j.ecoenv.2023.115475 (2023).
14. Lu, Q. et al. Deltamethrin toxicity: A review of oxidative stress and metabolism. *Environ. Res.* **170**, 260–281. https://doi.org/10.1016/j.envres.2018.12.045 (2019).
15. Yuan, X. et al. Acute deltamethrin exposure induces oxidative stress, triggers Endoplasmic reticulum stress, and impairs hypoxic resistance of crucian carp. *Comp. Biochem. Physiol. C Toxicol. Pharmacol.* **263**, 109508. https://doi.org/10.1016/j.cbpc.2022.109508 (2023).
16. Dong, Z. X. et al. Honeybee (Apis mellifera) resistance to deltamethrin exposure by modulating the gut microbiota and improving immunity. *Environ. Pollut.* **314**, 120340. https://doi.org/10.1016/j.envpol.2022.120340 (2022).
17. Li, T. et al. Deciphering the interplay between LPS/TLR4 pathways, neurotransmitter, and deltamethrin-induced depressive-like behavior: perspectives from the gut-brain axis. *Pestic Biochem. Physiol.* **197**, 105697. https://doi.org/10.1016/j.pestbp.2023.105697 (2023).
18. Zhong, C. et al. Intestinal microbiota and gene expression alterations in Chinese mitten crab (Eriocheir sinensis) under deltamethrin exposure. *Antioxid. (Basel).* 14. https://doi.org/10.3390/antiox14050510 (2025).
19. Lin, S. P. et al. Applications of atmospheric cold plasma in agricultural, medical, and bioprocessing industries. *Appl. Microbiol. Biotechnol.* **106**, 7737–7750. https://doi.org/10.1007/s00253-022-12252-y (2022).
20. Katsigiannis, A. S., Bayliss, D. L. & Walsh, J. L. Cold plasma for the disinfection of industrial food-contact surfaces: an overview of current status and opportunities. *Compr. Rev. Food Sci. Food Saf.* **21**, 1086–1124. https://doi.org/10.1111/1541-4337.12885 (2022).
21. Sun, T. et al. Plasma-Activated solutions mitigates DSS-Induced colitis via restoring redox homeostasis and reversing microbiota dysbiosis. *Adv. Sci. (Weinh).* **10**, e2304044. https://doi.org/10.1002/advs.202304044 (2023).
22. Bekeschus, S. Medical gas plasma technology: roadmap on cancer treatment and immunotherapy. *Redox Biol.* **65**, 102798. https://doi.org/10.1016/j.redox.2023.102798 (2023).
23. Ezzatpanah, H. et al. New food safety challenges of viral contamination from a global perspective: Conventional, emerging, and novel methods of viral control. *Compr. Rev. Food Sci. Food Saf.* **21**, 904–941. https://doi.org/10.1111/1541-4337.12909 (2022).
24. O'Connor, N., Cahill, O., Daniels, S., Galvin, S. & Humphreys, H. Cold atmospheric pressure plasma and decontamination. Can it contribute to preventing hospital-acquired infections? *J. Hosp. Infect.* **88**, 59–65. https://doi.org/10.1016/j.jhin.2014.06.015 (2014).
25. Konturek, P. C. et al. Participation of the intestinal microbiota in the mechanism of beneficial effect of treatment with synbiotic syngut on experimental colitis under stress conditions. *J. Physiol. Pharmacol.* **71** https://doi.org/10.26402/jpp.2020.3.03 (2020).
26. Jung, J. M. et al. Anticancer effect of cold atmospheric plasma in syngeneic mouse models of melanoma and colon cancer. *Molecules* **28** https://doi.org/10.3390/molecules28104171 (2023).
27. Wu, Z. et al. Plasma-Activated AVC hydrogel for reactive oxygen and nitrogen species delivery to treat allergic contact dermatitis. *ACS Appl. Mater. Interfaces*. **16**, 58379–58391. https://doi.org/10.1021/acsami.4c14006 (2024).
28. Ma, Y. et al. Plasma-activated solutions prevent peritoneal adhesion formation by regulating eNOS expression in mesothelial cells. *J. Adv. Res.* https://doi.org/10.1016/j.jare.2025.02.024 (2025).
29. Feriani, A. et al. HPLC-DAD-ESI-QTOF-MS/MS profiling of zygophyllum album roots extract and assessment of its cardioprotective effect against deltamethrin-induced myocardial injuries in rat, by suppression of oxidative stress-related inflammation and apoptosis via NF-κB signaling pathway. *J. Ethnopharmacol.* **247**, 112266. https://doi.org/10.1016/j.jep.2019.112266 (2020).
30. Hossain, M. M., Toltin, A. C., Gamba, L. M. & Molina, M. A. Deltamethrin-Evoked ER Stress Promotes Neuroinflammation in the Adult Mouse Hippocampus. *Cells* 11, https://doi.org/10.3390/cells11121961 (2022).
31. Wu, H. et al. Histopathology and transcriptome analysis reveals the gills injury and immunotoxicity in Gibel carp following acute deltamethrin exposure. *Ecotoxicol. Environ. Saf.* **234**, 113421. https://doi.org/10.1016/j.ecoenv.2022.113421 (2022).

32. Ma, L. et al. Cold atmospheric plasma alleviates radiation-induced skin injury by suppressing inflammation and promoting repair. *Free Radic Biol. Med.* **204**, 184–194. https://doi.org/10.1016/j.freeradbiomed.2023.05.002 (2023).
33. Mekircha, F. et al. Early-Life exposure to commercial formulation containing deltamethrin and Cypermethrin insecticides impacts redox system and induces unexpected regional effects in rat offspring brain. *Antioxid. (Basel)*. **12** https://doi.org/10.3390/antiox12051047 (2023).
34. Fang, Z. et al. Integration of metabolomics and transcriptomics reveals the toxicological mechanism of deltamethrin exposure in Chinese mitten crab eriocheir sinensis. *Sci. Total Environ.* **955**, 176975. https://doi.org/10.1016/j.scitotenv.2024.176975 (2024).
35. Han, Y., Zhang, Q., Chen, L., Zhao, J. & Yang, D. In vitro study of deltamethrin-induced extracellular traps in hemocytes of ruditapes philippinarum. *Ecotoxicol. Environ. Saf.* **256**, 114909. https://doi.org/10.1016/j.ecoenv.2023.114909 (2023).
36. Bourdens, M. et al. Short exposure to cold atmospheric plasma induces senescence in human skin fibroblasts and adipose mesenchymal stromal cells. *Sci. Rep.* **9**, 8671. https://doi.org/10.1038/s41598-019-45191-2 (2019).
37. Dai, X., Lv, X. & Xi, M. Cold atmospheric plasma targets triple negative breast cancer cells via SCAF11-mediated competitive protein degradation and synergizes with miRNA-146b-5p. *Int. J. Biol. Macromol.* **312**, 144142. https://doi.org/10.1016/j.ijbiomac.2025.144142 (2025).
38. Dai, X., Feng, S. & Li, T. Cold atmospheric plasma control metabolic syndromes via targeting fat mass and obesity-associated protein. *Pharmacol. Res.* **215**, 107720. https://doi.org/10.1016/j.phrs.2025.107720 (2025).
39. Wu, P. S. et al. Cold atmospheric plasma jet promotes wound healing through CK2-Coordinated PI3K/AKT and MAPK signaling pathways. *Mol. Cell. Proteom.* **24**, 100962. https://doi.org/10.1016/j.mcpro.2025.100962 (2025).
40. Zhang, N. et al. Controlled release of cold atmospheric plasma by gelatin scaffold enhances wound healing via macrophage modulation. *ACS Appl. Mater. Interfaces.* **17**, 15050–15066. https://doi.org/10.1021/acsami.4c21635 (2025).
41. Zheng, Y. et al. Next-Generation oral ulcer management: integrating cold atmospheric plasma (CAP) with Nanogel-Based pharmaceuticals for inflammation regulation. *Adv. Healthc. Mater.* **14**, e2403223. https://doi.org/10.1002/adhm.202403223 (2025).
42. Artamonov, M. Y., Pyatakovich, F. A. & Minenko, I. A. Synergistic antioxidant effects of molecular hydrogen and cold atmospheric plasma in enhancing mesenchymal stem cell therapy. *Antioxid. (Basel)*. 13. https://doi.org/10.3390/antiox13121584 (2024).
43. Sardella, E. et al. Plasma treated water solutions in cancer treatments: the contrasting role of RNS. *Antioxid. (Basel)*. **10** https://doi.org/10.3390/antiox10040605 (2021).
44. Pang, B. et al. Enhanced anticancer efficacy of alkaline Plasma-Activated water through augmented RONS production. *ACS Appl. Mater. Interfaces*. **17**, 467–483. https://doi.org/10.1021/acsami.4c16518 (2025).
45. Zhou, Y. et al. Changes to pork bacterial counts and composition after dielectric barrier discharge plasma treatment and storage in Modified-Atmosphere packaging. *Foods* **13** https://doi.org/10.3390/foods13244162 (2024).
46. Los, A. et al. Improving Microbiological safety and quality characteristics of wheat and barley by high voltage atmospheric cold plasma closed processing. *Food Res. Int.* **106**, 509–521. https://doi.org/10.1016/j.foodres.2018.01.009 (2018).
47. Yu, W. et al. Cold atmospheric plasma enhances immune clearance of Porphyromonas gingivalis via LC3-associated phagocytosis in mice with experimental periodontitis. *Int. Immunopharmacol.* **153**, 114494. https://doi.org/10.1016/j.intimp.2025.114494 (2025).
48. Meinke, M. C. et al. Radical formation in skin and preclinical characterization of a novel medical plasma device for dermatology after single application. *Free Radic Biol. Med.* **226**, 199–215. https://doi.org/10.1016/j.freeradbiomed.2024.11.026 (2025).
49. Manzhula, K., Rebl, A., Budde-Sagert, K. & Rebl, H. Interplay of cellular Nrf2/NF-κB signalling after plasma stimulation of malignant vs. Non-Malignant dermal cells. *Int. J. Mol. Sci.* **25** https://doi.org/10.3390/ijms252010967 (2024).
50. Kyi, P. et al. Endothelial senescence mediates hypoxia-induced vascular remodeling by modulating PDGFB expression. *Front. Med. (Lausanne)*. **9**, 908639. https://doi.org/10.3389/fmed.2022.908639 (2022).

Author contributions

Xiaoyuan Deng: Data curation, Writing – original draft. Tuanhe Sun: Funding acquisition, Writing – review & editing. Siyi Wang: Formal analysis, Methodology. Kaijie Ren: Formal analysis, Methodology. Tianhao Min: Methodology, Software. Yuyi Ma: Formal analysis, Methodology. Yuanchang Peng: Data curation. Xueni Wang: Data curation, Methodology. Bo Zhang: Data curation, Methodology. Yanglong Nan: Data curation. Shiyao Tong: Data curation. Yuanyuan Liu: Data curation. Wei Wang: Data curation, Visualization. Yong Zhang: Validation, Software, Methodology, Investigation. Yong Yang: Validation, Software, Methodology, Investigation. Kang Li: Writing – review & editing. Chengxue Dang: Supervision, Writing – review & editing. Hao Zhang: Funding acquisition, Supervision, Writing – review & editing. Kun Zhu: Funding acquisition, Writing – review & editing.

Funding

This work was supported by the Fundamental Research Funds for the Central Universities (No. xzy012024115), the Clinical Research Award of the First Affiliated Hospital of Xi' an Jiaotong University, China (No. XJTU-1AF-CRF-2023-034), the Natural Science Basic Research Program of Shaanxi (Program No.2025JC-YBQN-1236) and the Clinical Research Award of the First Affiliated Hospital of Xi'an Jiaotong University, China (No. 2024-MS-18).

Declarations

Competing interests

The authors declare no competing interests.

Ethics approval

All animal experiments in this study complied with the ethical guidelines for animal experiments and the conduct of animal experiments was supervised and approved by the Institutional Animal Care Committee of the Animal Experimental Centre of Xi' an Jiaotong University (ethical approval number: No. 2024 – 1803) and was reported in accordance with the ARRIVE guidelines.

Additional information

Supplementary Information The online version contains supplementary material available at https://doi.org/10.1038/s41598-025-32475-z.

Correspondence and requests for materials should be addressed to H.Z. or K.Z.